Tropical Gravity Waves and Superclusters Simulated by High-Horizontal-Resolution SKYHI General Circulation Models

By Y. Hayashi, D.G. Golder

Geophysical Fluid Dynamics Laboratory/NOAA, Princeton University
P. O. Box 308, Princeton, New Jersey 08542, USA

and

P.W. Jones

Theoretical Division T-3 MS B216, Los Alamos National Laboratory
Los Alamos, New Mexico 87544, USA

(Manuscript received 5 June 1997, in revised form 13 October 1997)

Abstract

Tropical gravity waves and superclusters simulated by 40-level GFDL SKYHI general circulation model experiments with higher horizontal resolutions (0.6° longitude × 0.72° latitude) and (1.0° × 1.2°) are compared with those simulated by a lower-resolution (3.0° × 3.6°) experiment.

Results indicated that simulated precipitational heating appears to excite tropical gravity waves. At higher resolutions, precipitation is more confined in space and time, resulting in a broader wavenumber-frequency spectral distribution. Grid-scale precipitation, which is thought to mimic the precipitation associated with cloud clusters, is organized into larger-scale superclusters. The westward propagation of cloud clusters and eastward propagation of superclusters can be more clearly seen in the high-resolution experiments.

The high-resolution (0.6° × 0.72°) model indicates that the lower-stratospheric gravity-wave momentum flux is dominated by high-frequency components having periods shorter than one day. This flux doubles as the resolution is increased from (3.0° × 3.6°) to (0.6° × 0.72°). It is speculated that a further increase in both the horizontal and vertical resolutions could substantially enhance the gravity-wave momentum flux convergence, thus forcing a stronger quasi-biennial oscillation.

1. Introduction

In previous papers (Hayashi *et al.*, 1984, 1989; Miyahara *et al.*, 1986; Hamilton and Mahlman, 1988; Hayashi and Golder, 1994), tropical gravity waves appearing in the GFDL "SKYHI" general circulation model were analyzed with respect to their wavenumber-frequency spectral distribution, structure, and propagation. The simulated gravity waves consisted of eastward- and westward-moving components having comparable magnitudes for periods of less than two days and wavenumbers greater than five.

In particular, Hayashi and Golder (1994) demonstrated that the 40-level SKYHI model with a horizontal resolution of N30 (3.0° latitude × 3.6° longitude) adequately simulated stratospheric

Kelvin waves (Wallace and Kousky 1968) and mixed Rossby-gravity (MRG) waves (Yanai and Maruyama, 1966), concurring with the same conclusions (Boville and Randel 1992) based on an NCAR model. These waves had been theoretically assumed (*e.g.*, Holton and Lindzen, 1972) to be the primary momentum forcing of the observed (Reed *et al.*, 1961) quasi-biennial oscillation (QBO) of the equatorial stratospheric zonal wind. The QBO simulated by the N30 SKYHI model, however, was one order of magnitude weaker than that observed (Hamilton *et al.*, 1995). It was then speculated (Hayashi and Golder, 1994) that this weak QBO could be substantially enhanced by small-scale gravity waves which were not resolved by the N30 model. Although gravity waves were originally assumed to force the QBO in the first theory of QBO (Lindzen and Holton, 1968), this assumption had not been accepted, since

gravity waves were not observed in the tropics at that time.

On the other hand, Maruyama (1994) and Sato et al. (1994) demonstrated that the vertical momentum flux associated with observed gravity waves in the period range of 1–3 days was synchronized with the QBO. Since oscillations having periods shorter one day were not resolved by the twice-daily sampled wind and temperature data used in their analyses, the 1–3-day momentum flux diagnostically estimated from these data could be severely underestimated, as suggested by Sato (1977).

Other observational and numerical studies (e.g., Pfister et al., 1993; Bergman and Salby, 1994; Mengel et al., 1995; Alexander and Holton, 1997; Dunkerton, 1997) also suggest that the meso-scale gravity-wave flux could substantially contribute to the QBO. An updated review of equatorial gravity-wave momentum flux can be found in Dunkerton (1997).

Recently, the SKYHI model has been integrated at a much higher resolution of N150 ($0.6° \times 0.72°$) for model months of May and June at the Los Alamos National Laboratory (see Jones et al., 1997 for the simulated climatology). The present study analyzed tropical gravity waves and superclusters simulated by the N150 model during June and compares the results with those from the N30 and N90 ($1.0° \times 1.2°$) models integrated at GFDL. Preliminary results from the N30 and N90 models have been presented in Hayashi and Golder (1994). Section 2 describes the model data and wave analyses. Section 3 summarizes the results and discusses the implications for the role that the gravity-momentum flux plays in the QBO.

2. Wave analyses

2.1 Model data

The general circulation models analyzed in the present study are the 40-level "SKYHI" models extending from the surface to about 0.01 mb (80 km) with a vertical resolution of about 1, 2, and 4 km in the troposphere, stratosphere, and mesosphere, respectively. These models have horizontal resolutions of N30 ($3.0°$ latitudes by $3.6°$ longitudes), N90 ($1.0° \times 1.2°$), and N150 ($0.6° \times 0.72°$). The model's physical processes include a scheme of moist convective adjustment (Manabe et al., 1965), surface hydrology, a planetary boundary layer, and radiation. Also included are orography, an imposed annual cycle of isolation, a climatological set of seasonal sea-surface temperatures, and climatological cloudiness. Neither the parameterized drag due to orographically forced gravity waves nor the diurnal cycle of solar insolation is incorporated. Details of the SKYHI model can be found in the papers of Fels et al. (1980), Levy et al. (1982), Hamilton and Mahlman (1988), Manzini and Hamilton (1993), and

Hamilton et al. (1995). Results obtained from this model have been described in the following papers: Mahlman and Sinclair (1980), Mahlman and Umscheid (1984, 1987), Andrews et al. (1983), Miyahara et al. (1986), Hamilton and Mahlman (1988), Hayashi et al. (1989), Manzini and Hamilton (1993), Hayashi and Golder (1993, 1994), Hamilton (1995), Hamilton et al. (1995), and Hamilton (1996, a review).

The simulated data analyzed are hourly data during June 6–July 4 sampled from the N30 and N150 models, in addition to the 3-hourly data sampled from the N90 model data used in Hamilton (1993) and Hayashi and Golder (1994). The model data are examined through a space-time spectral analysis (see Hayashi, 1982) using the lag-correlation method. The space-time power spectra and cospectra are "equatorially" averaged over the latitudinal bands of 10.5°–10.5°S for N30, 0.5°N–0.5°S for N90, and 0.9°N–0.9°S for N150. Although a rather wide equatorial band is used only for the N30 spectra to increase the statistical significance, the N30 spectra are found to be insensitive to a decrease in the latitudinal band width.

2.2 Precipitation and vertical velocity

Recently, Hayashi and Golder (1997a, b) numerically and theoretically examined several mechanisms for the generation of low- and high-frequency tropical waves simulated in an idealized model with moist convective adjustment. It was demonstrated that superclusters, as well as Kelvin and MRG waves, are maintained primarily through the "saturation-triggering mechanism" proposed by Hayashi and Golder (1994). This mechanism hypothesizes that several tropical transient waves are triggered by the intermittent onset of moist convection, upon saturation, to neutralize any pre-existing conditionally unstable stratification that has developed during periods of nonsaturation. The results from the idealized model suggested that tropical gravity waves could also be generated by this mechanism, although the horizontal resolution of the model was not sufficient to examine this possibility.

Since tropical gravity waves may be excited by the convective heating associated with vertical motion, precipitation and vertical velocity are first examined. Figure 1 shows the longitude-time distribution of three-hourly averaged N150 equatorial precipitational heating over 90°E–90°W during June 1–July 4. This figure reveals eastward-moving groups of westward-moving grid-scale oscillations. Figure 2 displays the longitude-time distributions at (a) N30, (b) N90, and (c) N150 of three-hourly averaged equatorial precipitational heating over 90°E to 90°W during June 6–16. It is seen that precipitation is more confined in space and time in the N150 and N90 models than in the N30 model.
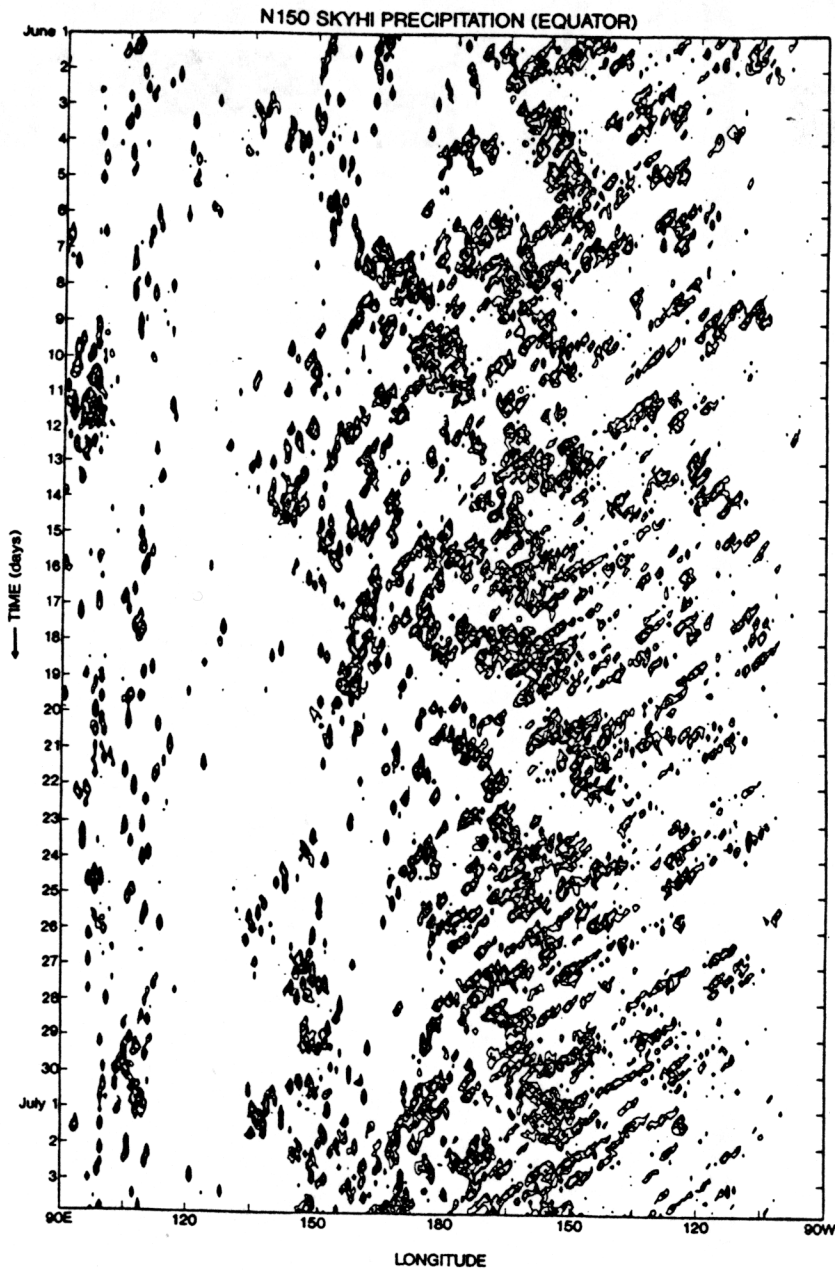
N150 SKYHI PRECIPITATION (EQUATOR)

Fig. 1. Equatorial longitude-time distribution of the N150 three-hourly averaged precipitational heating over 90°E–90°W during June 1–July 3. The contour values are 0.5, 1, 2, 5, 10, 20, 50, 100, and 200 (388 W m^{-2}).

Observed superclusters (Nakazawa, 1988, 1995; Hayashi and Nakazawa, 1989; Mapes and Houze, 1993; Chen *et al.*, 1996) are associated with a half-wavelength of 2000–4000 km and periods of 5–15 days, propagating eastward with phase speeds of 5–10 ms^{-1}. They consist of several smaller-scale (half-wavelength of 100–500 km) cloud clusters that propagate westward. Recently, Takayabu (1994a, b) observationally interpreted the westward-moving quasi-two-day cloud clusters as westward-moving equatorial inertio-gravity waves. The westward-propagation of grid-scale precipitation, which is thought to mimic cloud clusters, and the eastward-propagation of superclusters can be more clearly seen in the N90 and N150 models (Figs. 2b and 2c) than in the N30 model (Fig. 2a), although these propagations are not as clear as those observed.

Figure 3 shows the wavenumber-frequency distributions (a) N30, (b) N90, and (c) N150 of the equatorially averaged power spectra of precipitational heating. The precipitational heating spectra, characterized by eastward- and westward-moving components of comparable magnitude, are associated with broader wavenumber-frequency distributions
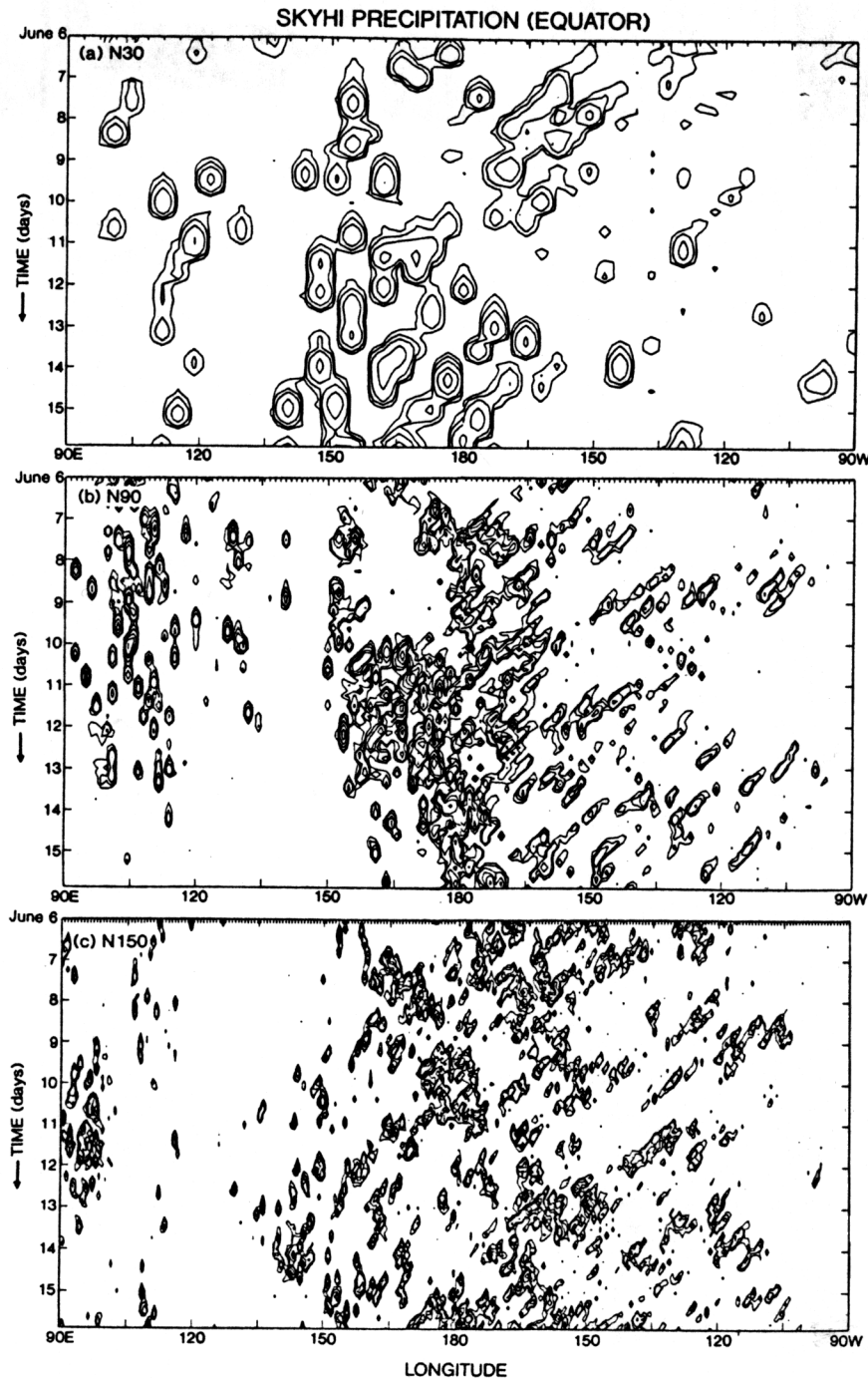
SKYHI PRECIPITATION (EQUATOR)

Fig. 2. Equatorial longitude-time distribution of the (a) N30 , (b) N90, and (c) N150 three-hourly averaged precipitational heating over 90°E–90°W during June 6–16. The contour values are 0.5, 1, 2, 5, 10, 20, 50, 100, and 200 (388 W m^{-2}).

at higher resolutions.

This figure (Fig. 3), however, does not reveal space-time spectral peaks corresponding to those (wavenumbers 11–21 and periods 1–3 days) of observed westward-moving equatorial cloud clusters estimated over an 80°E–160°W longitude span (Takayabu, 1994a, b), although the westward propagation of grid-scale precipitation can be seen in

the longitude-time section (Fig. 1). This probably results from the domain of the present space-time spectral analysis including longitude spans where the precipitation does not propagate. Moreover, spectral peaks corresponding to eastward-moving superclusters (wavenumber 5–10, period 10–20 days) are not seen, although their eastward propagation can be seen in Fig. 1. This is probably due
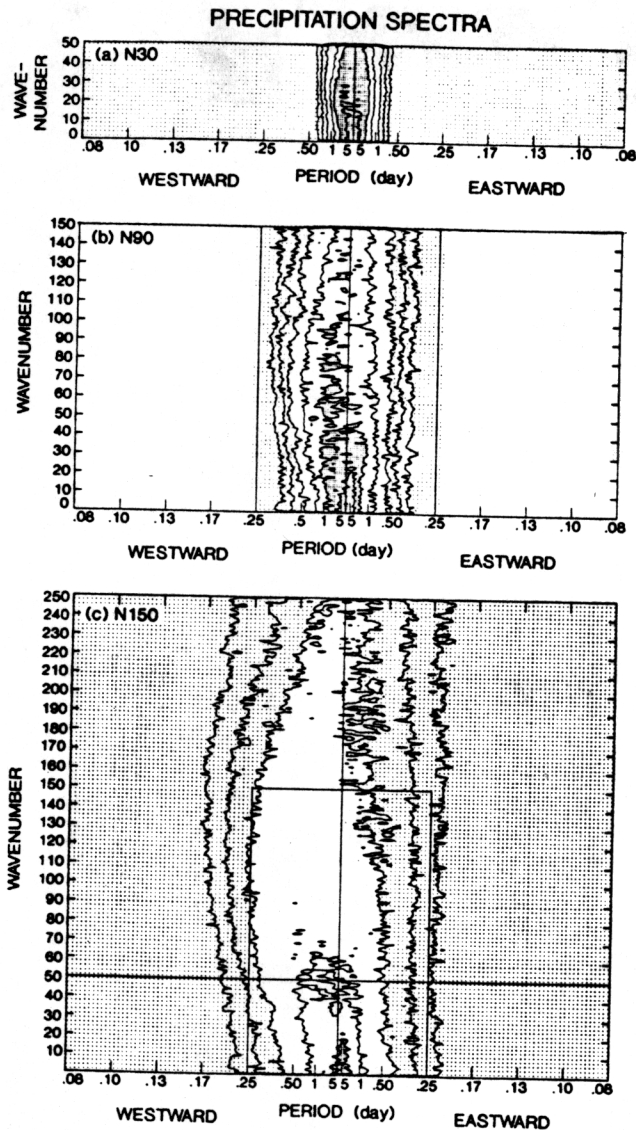
PRECIPITATION SPECTRA

Fig. 3. Wavenumber-frequency distributions of the equatorially averaged power spectra of the (a) N30, (b) N90, and (c) N150 precipitational heating in the range of wavenumber 0–250 and periods longer than 0.083 days that can be resolved by the hourly sampled N150 grid-point data. The inner domains indicate the range of wavenumbers and frequencies resolved by the (a) hourly sampled N30 grid-point data (wavenumbers 0–50, periods longer than 0.083 days) and (b) three-hourly sampled N90 grid-point data (wavenumbers 0–150, periods longer than 0.25 days). The contour values are 0.5, 1, 2, 5, and 10 (135 $W^2 m^{-4}$ day)

to the record length of 30 days being too short for the present spectral analysis technique to isolate superclusters.

Figures 4 and 5 show longitude-time distributions of the N150 upward and downward pressure-velocities, respectively. The 9.2-mb pressure-velocity field is dominated by gravity waves consisting of both upward (Fig. 4a) and downward (Fig. 5a) pressure-velocities. The upward 537-mb pressure-velocity (Fig. 4b) reveals eastward-moving superclusters consisting of grid-scale pulses of upward pressure-velocity. These upward velocities correspond to grid-scale pulses of precipitation (Fig. 2c). In contrast to the upward 537-mb pressure-velocity (Fig. 4b), the downward 537-mb pressure-velocity (Fig. 5b) exhibits much weaker grid-scale pulses. The superclusters are confined to the troposphere, whereas the gravity waves appear to propagate upward from the troposphere to the stratosphere.

Figures 6a and 6b show the wavenumber-frequency distributions of the equatorially averaged power spectra of the N150 pressure-velocity at 9.2 mb and 537 mb, respectively. The 537-mb pressure-velocity spectra are characterized by eastward- and westward-moving components of comparable magnitude, being biased toward the westward-moving component for wavenumbers 50–200. In contrast to the 537-mb spectra, the 9.2-mb spectra lack low-frequency components. This result is consistent with the fact that lower-frequency gravity waves theoretically have smaller vertical group velocities, and thus less efficiently propagate from troposphere.

2.3 Vertical momentum flux

Figure 7a, 7b and 7c show the wavenumber-frequency distributions of equatorially averaged cospectra of the N30, N90, and N150 vertical momentum fluxes at 9.2 mb (32 km), respectively. These spectral distributions are similar to the power spectral distribution of the 9.2-mb vertical pressure-velocity (Fig. 6a), except that the momentum-flux spectra allow negative as well as positive values. These spectra indicate that westward- and eastward-moving gravity waves transport easterly and westerly momentum, respectively. The slanted lines in the figures indicate a constant phase velocity of 30 ms^{-1}. It is seen that these spectra are associated with wider wavenumber and frequency distributions at higher resolutions. For the lower half of the resolvable wavenumbers, the dominant frequencies increase with wavenumber. This increase is consistent with theoretical nonrotating hydrostatic gravity waves, which have the same vertical wavenumber and the same phase velocity for different zonal wavenumbers (i.e., a constant ratio between frequency and zonal wavenumber). For the higher half of the resolvable wavenumbers, the dominant

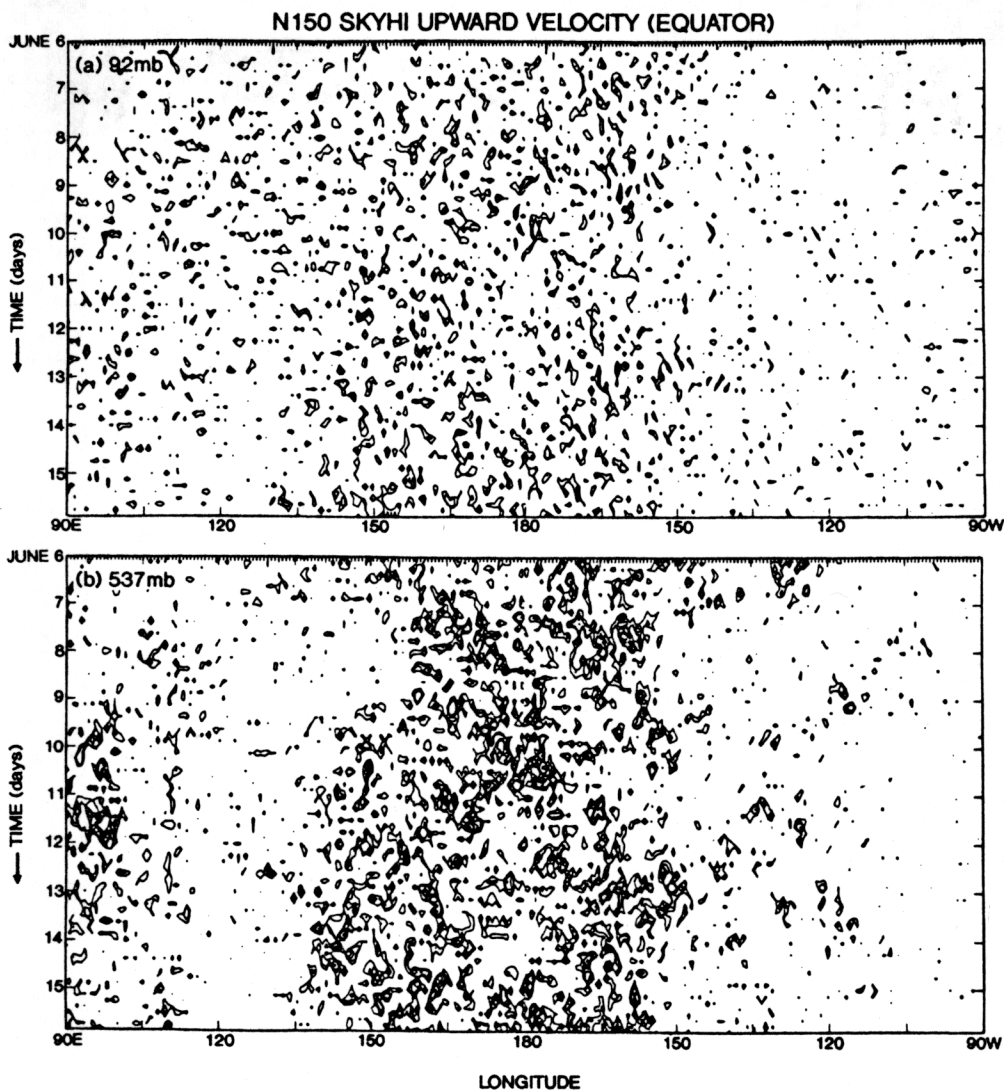**N150 SKYHI UPWARD VELOCITY (EQUATOR)**

Fig. 4. Equatorial longitude-time distributions of the N150 vertical pressure-velocity at (a) 9.2 mb and
(b) 537 mb. Contours are drawn only for upward velocity. The contour values are (a) 0.1, 0.2, and
0.5 (10^{-3} mb s^{-1}), and (b) 0.2, 0.5, 1, 2, and 5 (units 10^{-2} mb s^{-1}).

frequencies decreases with wavenumber, implying
lower phase speeds for the higher wavenumbers. It
was suggested (Hayashi et al., 1989, p. 429) that
the lower phase speeds are due to finite-difference
errors, since the phase speeds depend on horizontal
resolution.

Table 1 lists the height distributions of the equa-
torially averaged vertical momentum flux spectra for
the N30 model (wavenumbers 5–50) and N150 model
(wavenumbers 5–250), along with the ratio of the
N150 to N30 spectra. According to this table, the
stratospheric momentum flux and also its vertical
convergence (not indicated here) are twice as strong
in the N150 model as in the N30 model. The mo-
mentum flux reverses sign around the 5-km level.
The sign reversal theoretically implies that gravity-
wave energy propagates upward and downward from
its energy source in the middle troposphere.

2.4 Long- and short-period spectra

Table 2 lists the height distributions of the vertical
momentum flux for the N150 model (wavenumbers
5–250), partitioned into the long-period (1–30 days)
and short-period (0.08–1.0 day) components. Ac-
cording to this table, the short-period components
of the lower-stratospheric momentum flux and also
its vertical convergence (not indicated here) are one
order of magnitude stronger than the long-period
component. A large cancellation occurs between the
eastward- and westward-moving components, con-
sistent with the observed estimates of these compo-
nents by Sato and Dunkerton (1997).

Figure 8 and 9 compare the June equatorially av-
eraged time power spectra (60°E–120°E mean) of
N150 zonal (Fig. 8a) and meridional (Fig. 9a) ve-
locities with those observed (Figs. 8b and 9b) at
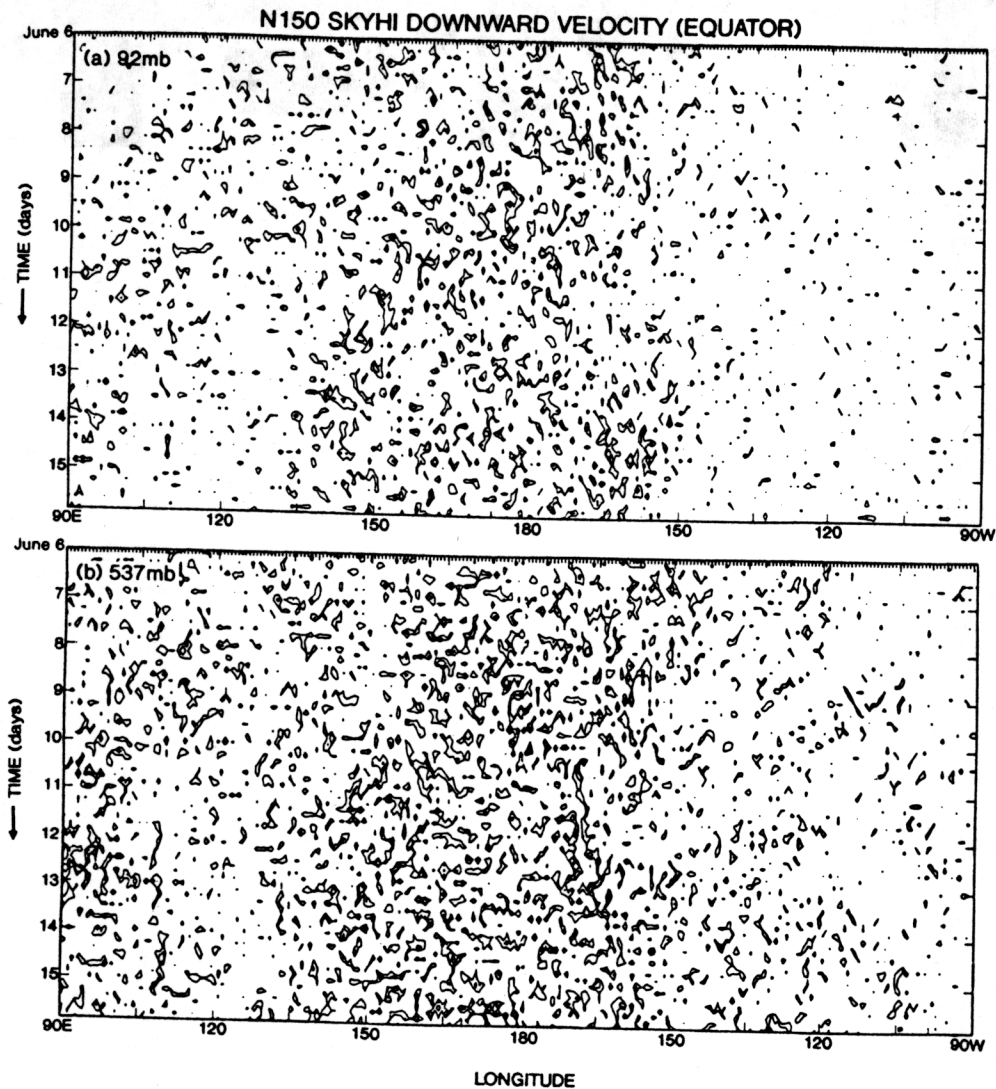Singapore (1°N, 104°E) during 1984–1993 (adapted

Fig. 5. As in Fig. 4, except that the contours are drawn only for downward velocity

from Sato *et al.*, 1994). The spectra have been multiplied by frequency. Since the observed data were sampled twice-daily, only the long-period (1–20 days) spectra are compared. The zonal-velocity spectra include 10–20-day Kelvin waves, while the meridional-velocity spectra include 3–5-day mixed Rossby-gravity waves. Both the observed and simulated spectra indicate that the long-period spectra are of the same magnitude. It should be noted that the SKYHI model has no diurnal cycle. Neither of these spectra, however, indicates any distinct spectral peak around 2–3-day periods. (Note that the light shading indicates weak values rather than strong values.) This result suggests that the observed 2–3-day oscillations (Maruyama, 1994; Sato *et al.*, 1994) are a small portion of gravity-wave spectra distributed over a wide range of periods.

2.5 Wavenumber-spectral distribution

Figure 10a shows the equatorially averaged stratospheric (47.9–104 mb mean) N150 transient vertical momentum flux as a function of zonal wavenumber in log-log coordinates. The wavenumber spectra have been smoothed over almost equal logarithmic intervals (see Table 3). It is seen that the momentum flux spectra (thick curve) fit the theoretical (Kraichnan, 1976) and observational (Gage, 1979) $-2/3$ power distribution (thin straight line) rather well for wavenumbers 50–250. The $-2/3$ power distribution for gravity-wave momentum flux is diagnostically consistent with a $-5/3$ power distribution of gravity-wave kinetic energy (see Hamilton, 1993, p. 170). The net momentum flux is found to fit the $-2/3$ power distribution better than the eastward- and westward-moving components (not
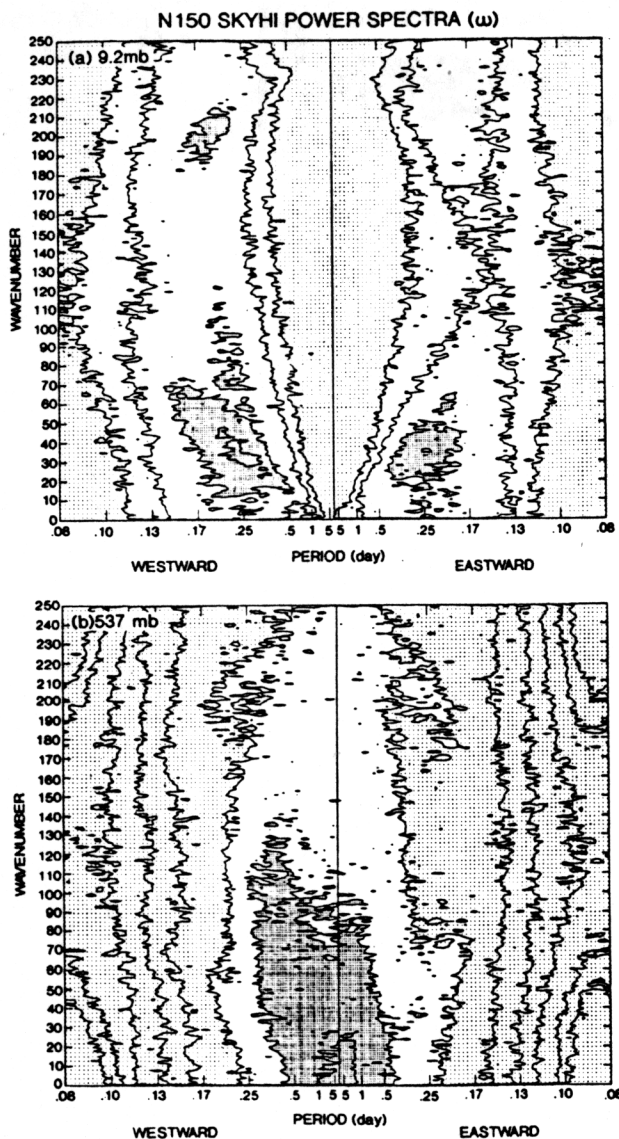
N150 SKYHI POWER SPECTRA (ω)

MOMENTUM FLUX SPECTRA

Fig. 6. Wavenumber-frequency distributions of equatorially averaged power spectra of the N150 vertical pressure-velocity at (a) 9.2 mb and (b) 537 mb. The contour values are (a) 1, 2, 5, and 10 (10^{-12} mb^2 s^{-2} day). Dark and light shadings indicate values greater than 5 and less than 1, respectively. In (b) the contour values are 1, 2, 5, 10, 20, 50, 100, and 200 (10^{-10} mb^2 s^{-2} day). Dark and light shadings indicate values greater than 100 and less than 50, respectively.
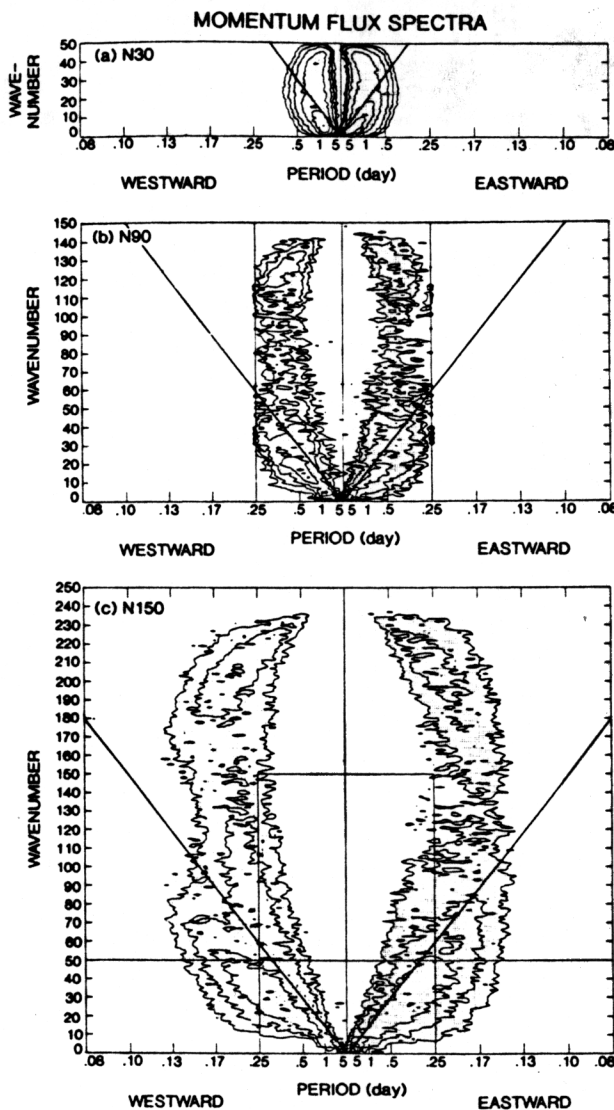
Fig. 7. Wavenumber-frequency distributions of equatorially averaged vertical momentum flux spectra for the (a) N30, (b) N90, and (c) N150 models at 9.2 mb. The slanted lines indicate constant 30 ms^{-1} phase velocity. The contour values are 0.5, 1, 2, 5, 10 and 20 (9.2 10^{-8} ms^{-1} mb s^{-1} day). Dark and light shadings indicate upward and downward fluxes, respectively.

illustrated). This is probably because these components can not accurately be separated for high wavenumber-frequency components, owing to the model's variables being discretized.

The spectral distribution curve in log-log coordinate representation gives the impression that the high-wavenumber components hardly contribute to the wavenumber-integrated momentum flux. The

area under the curve is, however, not proportional to the wavenumber-integrated momentum flux. To better visualize the wavenumber-integrated momentum flux, Fig. 10b displays the N150 vertical momentum flux spectra multiplied by wavenumber (thick solid line), plotted on a linear scale as a function of logarithmic wavenumber. The −2/3 power distribution curve multiplied by wavenumber (i.e., 1/3 power distribution) is indicated by the thin solid curve. The areas under the curves are now pro-

Table 1. Height distributions (June) of equatorially averaged vertical eddy momentum flux $-\overline{u'\omega'}$ (10^{-5} ms^{-1}·mb s^{-1}) associated with westward- and eastward-moving components consisting of zonal wavenumbers 5–50 (N30 model) and 5–250 (N150 model). The flux has been averaged over several levels. Positive and negative values indicate upward and downard fluxes, respectively. The right-hand columns indicate the ratio of the N150 to N30 flux.

level (km)	N30 ($5 \leq k \leq 50$)		N150 ($5 \leq k \leq 250$)		ratio (N150/N30)	
	westward	eastward	westward	eastward	westward	eastward
51–68	−0.4	1.4	−3.3	2.7	7.5	1.9
34–48	−1.9	2.9	−7.0	7.3	3.6	2.5
23–32	−4.4	6.8	−12.7	13.3	2.9	2.0
16–21	−6.6	11.0	−13.6	18.1	2.1	1.6
6.2–14	−7.0	8.3	−15.7	38.6	2.2	4.7
1.4–5.0	29.1	−34.8	85.1	−24.5	2.9	0.7

Table 2. Height distributions (June) of equatorially averaged N150 vertical momentum flux $-\overline{u'\omega'}$ (10^{-5} ms^{-1}·mb s^{-1}) associated with westward- and eastward-moving components consisting of zonal wavenumbers 5–250 in long-period (1–30 days) and short-period (0.08–1.0 days) ranges. The flux has been averaged over several levels. The right-hand columns indicate the ratio of the short-period to long-period flux.

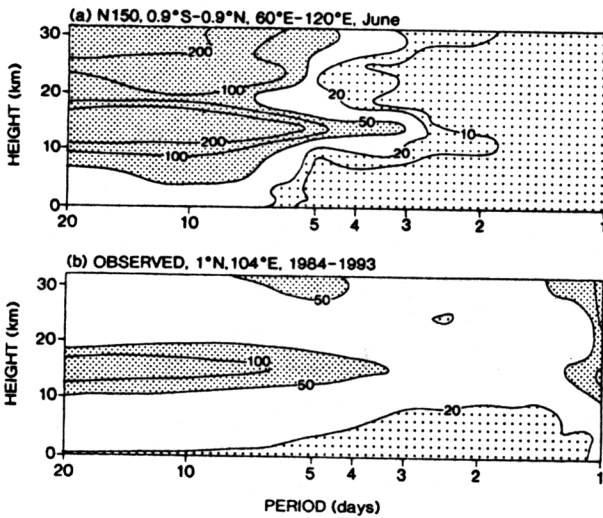| level (km)	long period		short period		ratio (short/long)	
	westward	eastward	westward	eastward	westward	eastward
51–68	−0.004	0.034	−3.3	2.7	825	79
34–48	−0.03	0.18	−7.0	7.1	233	39
23–32	−0.11	0.68	−12.5	12.6	114	19
16–21	0.23	1.8	−13.9	16.3	−60	9
6.2–14	5.6	7.4	−21.2	31.2	−4	4
1.4–5.0	11.5	−5.6	73.6	−18.9	6	3

TIME POWER SPECTRA (u)

Fig. 8. (a) Equatorially averaged time power spectra (60°E–120°E mean) of the N150 zonal velocity in June. (b) Time power spectra of the observed zonal velocity at Singapore (1°N, 104°E) during 1984–1993 (adapted from Sato *et al.* 1994). The spectra have been multiplied by frequency. Dark shade and light shadings indicate values greater than 50 and less than 10, respectively. The units are in (ms^{-1})^2.
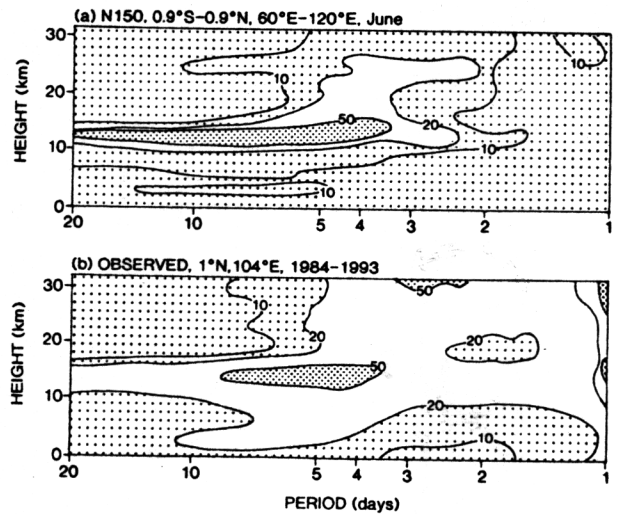
TIME POWER SPECTRA (v)
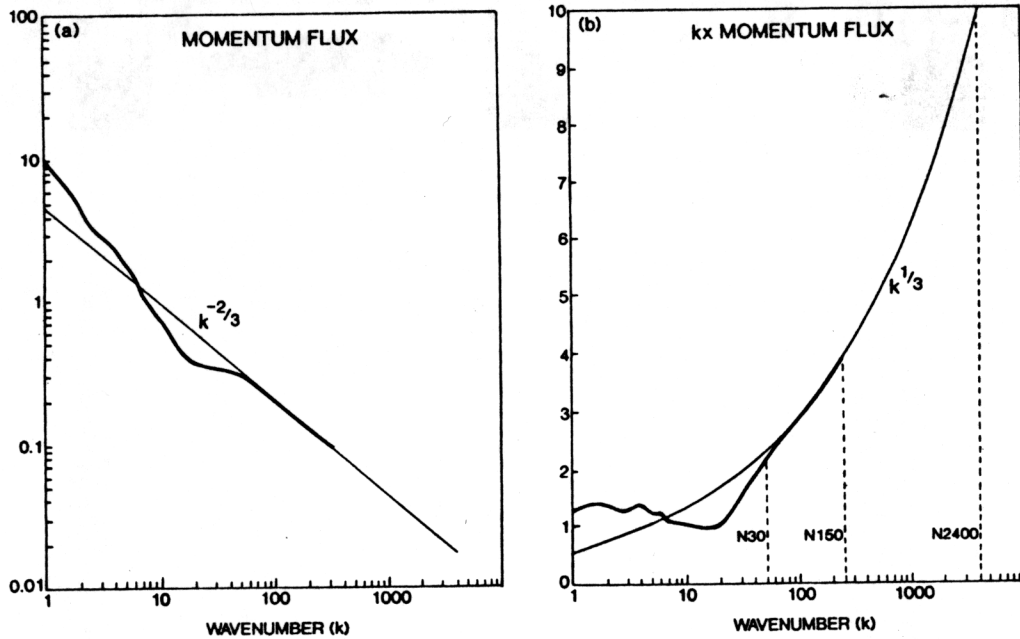

Fig. 9. As in Fig. 8, except for meridional velocity.

Fig. 10. (a) Equatorially averaged stratospheric (47.9–104 mb)-mean N150 transient vertical momentum flux spectra (ms^{-1} mb s^{-1}) plotted (thick solid curve) as a function of zonal wavenumber in log-log coordinates. The wavenumber spectra have been smoothed over equal logarithmic intervals (see Table 3). The thin solid line indicates the −2/3 power law distribution. (b) As in Fig. 10a, except that the spectra are multiplied by wavenumber and plotted (thick solid curve) in log-linear coordinates. The thin solid curve indicates the 1/3 power law distribution. The units are in 7.1 ms^{-1} mb s^{-1}.

Table 3. Ranges of zonal wavenumber (k) for the smoothing of wavenumber spectra by averaging over approximately equal intervals of log (k/2)–log (2k).

k	k/2 ∼ 2k
1	1–1
2	1–4
3	2–6
4	2–8
5	3–10
6	3–12
7	4–14
8	4–16
9	5–18
10	5–20
20	10–40
30	15–60
40	20–80
50	25–100
100	50–200
200	100–250

portional to the wavenumber-integrated momentum flux.

Theoretically (Jones, 1969), the horizontal wavelength must be greater than 10 km for the existence of internal gravity waves having a phase speed of 30 ms^{-1}, which is comparable to the equatorial stratospheric zonal velocity. This wavelength corresponds to wavenumber 4000, which can be resolved by an N2400 model. If it is assumed that the simulated gravity-wave momentum flux is distributed according to a −2/3 power law for wavenumbers 1–4000, the gravity-wave momentum flux should increase by a factor of two as the resolution is increased from N30 to N150, and an additional factor of three from N150 to N2400, as is demonstrated in Fig. 10b.

2.6 Oscillations in the monthly-mean zonal velocity

Figure 11 displays the equatorial time-height distributions of the composited monthly-mean zonal-mean zonal velocities for the (a) N30 and (b) N90 models. The monthly-mean zonal velocities have been annually composited over 10 and 2 years for the N30 and N90 models, respectively. These figures exhibit the downward propagation of the simulated semiannual oscillation (SAO) above 25 km, which had previously been detected (Hamilton and Mahlman, 1988; Hamilton et al., 1995) in the N30 model. The reader is referred to Hamilton et al. (1995) and Jones et al. (1997) for the latitude-

height distributions of zonal wind climatologies from the SKYHI models having various horizontal resolutions.

Figure 12a shows the equatorial time-height distribution of the N30 monthly-mean zonal-mean zonal velocity, exhibiting the downward propagation of the simulated mesospheric SAO over the 10-year period. Figure 12b is the same as Fig. 12a except that it displays the deviation from the 10-year composite, revealing the downward propagation of a weak stratospheric QBO, which had previously been detected (Hamilton et al., 1995) in the N30 model.

Figure 13 shows the equatorial frequency-height distributions of the time-power spectra of the monthly-mean zonal-mean zonal velocity of the (a) N30 model over a period of 10 years and (b) the N90 model over 2 years. Both the models exhibit spectral peaks at 6 and 12 months. Neither model, however, exhibits a QBO spectral peak isolated from the dominant annual peak. It is, therefore, not possible to determine whether the N90 model has a stronger QBO than the N30 model.

3. Summary and implications

Tropical gravity waves and superclusters simulated by 40-level GFDL SKYHI general circulation models with high horizontal resolutions of N150 (0.6° latitude × 0.72° longitude) and N90 (1.0° × 1.2°) were compared with those simulated by a lower-resolution N30 (3.0° × 3.6°) model.

Results indicate that precipitational heating appears to excite tropical gravity waves. For higher resolution, precipitation is more confined in space and time, resulting in a broader wavenumber-frequency spectral distribution. Gird-scale precipitation, which is thought to mimic precipitation associated with cloud clusters, is organized into superclusters. The westward propagation of cloud clusters and eastward propagation of superclusters are more clearly seen in the higher-resolution models, although these propagations are not as clear as observed.

The high-resolution (N150) model indicates that the lower-stratospheric gravity-wave momentum flux and its vertical convergence are dominated by high-frequency components having periods shorter than one day, although the high- and low-frequency components have comparable values of kinetic energy. This result suggests that observed gravity waves having periods shorter than one day may provide the principal source of momentum for the QBO. It also supports the suggestion (Sato, 1997) that the gravity-wave momentum flux diagnostically estimated from observed twice-daily samples wind and temperature data (Maruyama, 1994; Sato et al., 1994) could be severely underestimated.

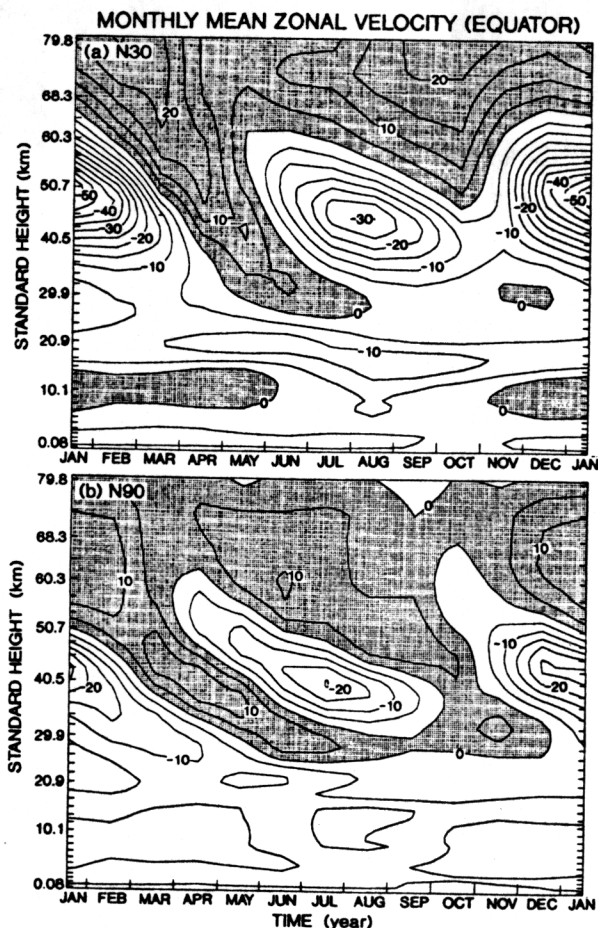The lower-stratospheric gravity-wave momentum flux and its vertical convergence are twice as strong

Fig. 11. Equatorial time-height distributions of the composited monthly-mean zonal-mean velocities of the (a) N30 and (b) N90 models. The monthly-mean zonal velocities have been annually composited over 10 and 2 years for the N30 and N90 models, respectively. The contour interval is 5 ms^{-1} and westerlies are shaded.

in the N150 model as in the N30 model. When $-5/3$ and $-2/3$ power wavenumber distributions are assumed over wavenumbers 1–4000 (wavelengths 10–40,000 km) for gravity-wave kinetic energy and vertical momentum flux, respectively, the gravity-wave momentum flux should increase by an additional factor of three as the horizontal resolution is further increased from N150 to N2400. The N30 model simulates only a very weak QBO (Hamilton et al., 1995). Since the stratospheric gravity-wave momentum flux convergence in the N150 model is twice as strong as that in the N30 model, it is expected that the QBO amplitude in the N150 model should be twice as strong as that in the N30 model. A further drastic increase in the horizontal resolution of the N150 model substantially enhance gravity-wave momentum flux convergence, thus forcing a stronger QBO.
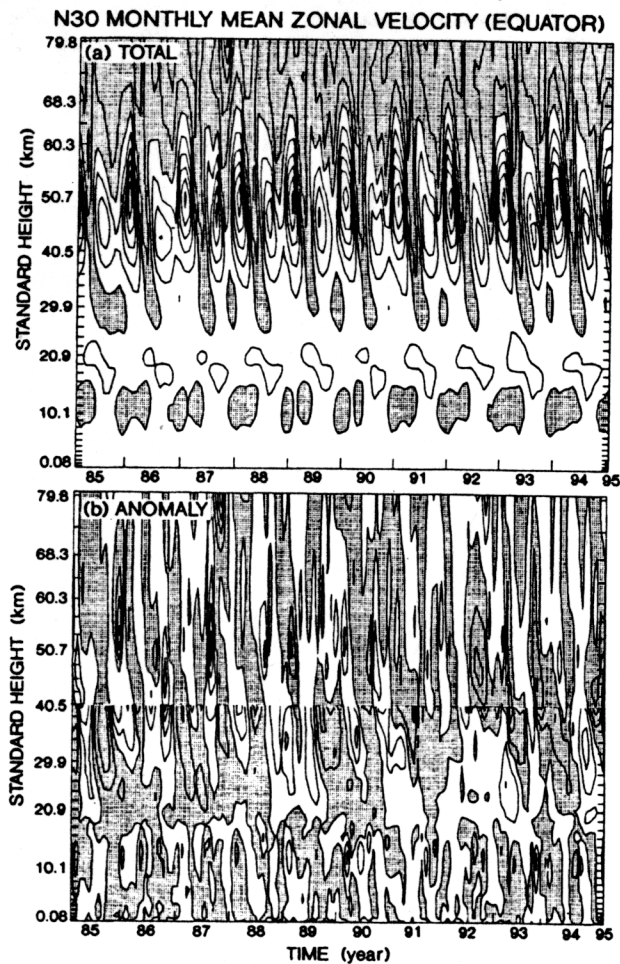
N30 MONTHLY MEAN ZONAL VELOCITY (EQUATOR)

Fig. 12. Equatorial time-height distributions of the (a) N30 monthly-mean zonal-mean zonal velocity and (b) its deviation from the 10-year composite. Westerlies are shaded. (a) The contour interval is 10 ms^{-1}. (b) The contour intervals are 6 ms^{-1} above 40 km and 2 ms^{-1} below 40 km.

TIME POWER SPECTRA (u), EQUATOR

Fig. 13. Equatorial frequency-height distributions of the time-power spectral density ($(ms^{-1})^2$ month) of the monthly-mean zonal-mean zonal velocity of the (a) N30 model over 10 years and (b) N90 model over 2 years. Dark and light shadings indicate values greater than 50 and less than 10, respectively. The contour values are 5, 10, 20, 50, 100, 200, 500, 1000, 2000, 5000, and 10000.

In an effort to examine the effect of the simulated gravity-momentum flux convergence on the simulated QBO amplitude, composite and time-spectral analyses were performed for the equatorial monthly-mean zonal-mean zonal velocity simulated by the N30 and N90 models. It was, however, not possible to determine whether the N90 model has a stronger QBO than the N30 model, since no QBO spectral peak isolated from the dominant annual cycle was found.

Recently, Takahashi (1996) demonstrated, using a low-horizontal resolution (T21) general circulation model with moist convective adjustment, that a fairly realistic QBO having a period of about 1.5 years can be simulated when the vertical resolution is as high as 0.5 km and the horizontal diffusion coefficient is one order of magnitude weaker than the conventional value. In this model, Kelvin and
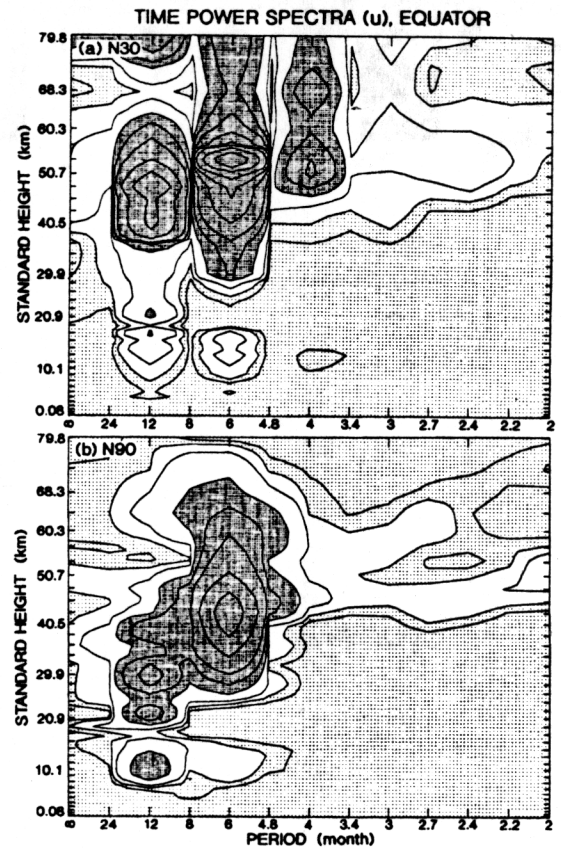
gravity waves play a major role in the momentum forcing of the QBO (Takahashi et al., 1997). The horizontal diffusion coefficient used in the SKYHI models decreases with grid size, being one order of magnitude weaker in the N90 model than in the N30 model. There is the possibility, therefore, that even the N90 model could simulate a strong QBO, if the vertical resolution is sufficiently increased to resolve short-vertical-scale gravity waves approaching their critical levels. In addition, increased vertical resolution will result in less inconsistency between the horizontal and vertical resolutions, as discussed by Lindzen and Fox-Rabinovitz (1989). The effect of increasing the vertical resolution of the N90 model on the gravity-wave momentum flux and the simulated QBO is being investigated.

Acknowledgments

References

Alexander, M.J. and J.R. Holton, 1997: A model study of zonal forcing in the equatorial stratosphere by convectively induced gravity waves. *J. Atmos. Sci.*, **54**, 408–419.

Andrews, D.G., J.D. Mahlman and R.W. Sinclair, 1983: Eliassen-Palm diagnostics of wave-mean flow interaction in the GFDL "SKYHI" general circulation model. *J. Atmos. Sci.*, **40**, 2768–2784.

Bergman, J.W. and M.L. Salby, 1994: Equatorial wave activity derived from fluctuations in observed convection. *J. Atmos. Sci.*, **51**, 3791–3806.

Boville, B.A. and W.J. Randel. 1992: Equatorial waves in a stratospheric GCM: Effects of vertical resolution. *J. Atmos. Sci.*, **49**, 785–801.

Chen, S.-S., R.A. Houze Jr. and B.E. Mapes, 1996: Multiscale variability of deep convection in relation to large-scale circulation in TOGA COARE. *J. Atmos. Sci.*, **53**, 1380–1409.

Dunkerton, T.J., 1997: The role of gravity waves in the quasi-biennial oscillation. *J. Geophys. Res.*, CADER issue (in press).

Fels, S.B., J.D. Mahlman, M.D. Schwarzkopf, and R.W. Sinclair, 1980: Stratospheric sensitivity to perturbations in ozone and carbon dioxide: Radiation and dynamical response. *J. Atmos. Sci.*, **37**, 2265–2297.

Gage, K.S., 1979: Evidence for a $k - 5/3$ law inertial range in mesoscale two-dimensional turbulence. *J. Atmos. Sci.*, **36**, 1950–1954.

Hamilton, K., 1993: What we can learn from the general circulation models about the spectrum of middle atmospheric motions. Coupling Processes in the Lower and Middle Atmosphere, Kluwer Academic Publishers, Netherlands, 161–174.

Hamilton, K., 1995: Interannual variability in the Northern Hemisphere winter middle atmosphere in control and perturbed experiments with the GFDL SKYHI general circulation model. *J. Atmos. Sci.*, **52**, 44–66.

Hamilton, K., 1996: Comprehensive meteorological modeling of the middle and upper atmosphere: A tutorial review. *J. Atmos. Terrestrial Physics*, **58**, 1591–1628.

Hamilton, K. and J.D. Mahlman, 1988: General circulation model simulation of the semiannual oscillation of the tropical middle atmosphere. *J. Atmos. Sci.*, **45**, 3212–3235.

Hamilton, K., R.J. Wilson, J.D Mahlman and L.J. Umscheid, 1995: Climatology of the SKYHI troposphere-stratosphere-mesosphere general circulation model. *J. Atmos. Sci.*, **52**, 5–43.

Hayashi, Y., 1982: Space-time spectral analysis and its applications to atmospheric waves. *J. Meteor. Soc. Japan*, **60**, 156–171.

Hayashi, Y. and D.G. Golder, 1993: Tropical 40–50 and 25–30 day oscillations appearing in realistic and idealized GFDL climate models and the ECMWF dataset. *J. Atmos. Sci.*, **50**, 464–494.

Hayashi, Y. and D.G. Golder, 1994: Kelvin and mixed Rossby-gravity waves appearing in the GFDL "SKYHI" general circulation model and the FGGE dataset: Implications for their generation mechanism and role in the QBO. *J. Meteor. Soc. Japan*, **72**, 901–935.

Hayashi, Y. and D.G. Golder, 1997a: United mechanisms for the generation of low- and high-frequency tropical waves. Part I: Control experiments with moist convective adjustment. *J. Atmos. Sci.*, **54**, 1262–1276.

Hayashi, Y. and D.G. Golder, 1997b: United mechanisms for the generation of low- and high-frequency tropical waves. Part II: Theoretical interpretations. *J. Meteor. Soc. Japan*, **75**, 775–797.

Hayashi, Y., D.G. Golder and J.D. Mahlman, 1984: Stratospheric and mesospheric Kelvin waves simulated by the GFDL "SKYHI" general circulation model. *J. Atmos. Sci.*, **41**, 1971–1984.

Hayashi, Y., D.G. Golder, J.D. Mahlman and S. Miyahara, 1989: The effect of horizontal resolution on gravity waves simulated by the GFDL SKYHI general circulation model. *Pure Appl. Geophys.*, **130**, 421–443.

Hayashi, Y.-Y. and T. Nakazawa, 1989: Evidence of the existence and eastward motion of superclusters at the equator. *Mon. Wea. Rev.*, **117**, 236–243.

Holton J.R. and R.S. Lindzen, 1972: An updated theory for the quasi-biennial cycle of the tropical stratosphere. *J. Atmos. Sci.*, **29**, 1076–1080.

Jones, W.L., 1969: Ray tracing for internal gravity waves. *J. Geophys. Res.*, **74**, 2028–2033.

Jones, P.W., K. Hamilton and R.J. Wilson, 1997: A very high-resolution general circulation model simulation of the global circulation in Austral winter. *J. Atmos. Sci.*, **54**, 1109–1116.

Kraichnan, R.H., 1976: Eddy viscosity in two and three dimensions. *J. Atmos. Sci.*, **33**, 1521–1536.

Levy, H.H., J.D. Mahlman and W.J. Moxim, 1982: Tropospheric N20 variability *J. Geophys. Res.*, **87**, 3061–3080.

Lindzen, R.S. and J.R. Holton, 1968: A theory of the quasi-biennial oscillation. *J. Atmos. Sci.*, **25**, 1095–1107.

Lindzen, R.S. and M. Fox-Rabinovitz, 1989: Consistent vertical and horizontal resolution. *Mon. Wea. Rev.*, **117**, 2575–2583.

Mahlman, J.D. and R.W. Sinclair, 1980: Recent results from the GFDL troposphere-stratosphere-mesosphere general circulation model. *Collection of Extended Abstracts Presented at ICMUA Sessions and IUGG Symposium 18*, IAMAP, Boulder, 11–18.

Mahlman, J.D. and L.J. Umscheid, 1984: Dynamics of the middle atmosphere: Success and problems of the GFDL "SKYHI" general circulation model. *Dynamics of the Middle Atmosphere*, J.R. Holton and T. Matsuno, Edts. Terra Scientific, 501–525.

Mahlman, J.D. and L.J. Umscheid, 1987: Comprehensive modeling of the middle atmosphere. The influence of horizontal resolution. *Transport Processes in*

the Middle Atmosphere, G. Visconti and R. Garcia, Eds., E. Reidel, 251–266

Manabe, S., J. Smagorinsky and R.F. Strictler, 1965: Simulated climatology of a general circulation model with a hydrologic cycle. Mon. Wea. Rev., 93, 769–798.

Manzini, E. and Hamilton, 1993: Middle atmospheric traveling waves forced by latent heat and convective heating. J. Atmos. Sci., 50, 2180–2200.

Mapes, B.E. and R.A. Houze, Jr., 1993: Cloud clusters and superclusters over the oceanic warm pool. Mon. Wea. Rev., 121, 1398–1415.

Maruyama T., 1994: Upward transport of westerly momentum due to disturbances of the equatorial lower stratosphere in the period range of about 2 days– A Singapore data analysis for 1983–1993. J. Meteor. Soc. Japan, 72, 423–432.

Mengel, J.G., H.G. Mayr, K.L. Chan, C.O. Hines, C.A. Reddy, N.F. Arnold and H.S. Porter, 1995: Equatorial oscillations in the middle atmosphere generated by small-scale gravity waves. Geophys. Res. Lett., 22, 3027–3030.

Miyahara, S., Y. Hayashi and J.D. Mahlman, 1986: Interaction between gravity waves and planetary-scale flow simulated by the GFDL SKYHI general circulation model. J. Atmos. Sci., 43, 1844–1861.

Nakazawa, T., 1988: Tropical super clusters within intraseasonal variations over the western Pacific. J. Meteor. Soc. Japan, 66, 823–839.

Nakazawa, T., 1995: Intraseasonal oscillations during the TOGA-COARE IOP. J. Meteor. Soc. Japan, 73, 305–319.

Pfister, L., K.R. Chan, T.P. Bui, S. Bowen, M. Legg, B. Gary, K. Kelly, M. Proffitt and W. Starr, 1993: Gravity waves generated by a tropical cyclone during the STEP tropical field program: a case study. J. Geophys. Res., 98, 8611–8638.

Reed, R.J., W.J. Campbell, L.A. Rasmussen and D.G. Rogers, 1961: Evidence of a downward-propagating annual wind reversal in the equatorial stratosphere. J. Geophys. Res., 66, 813–818.

Sato, K., 1997: Observational studies of gravity waves associated with convection. Gravity Wave Processes, NATO ASI Series, edited by K. Hamilton, 1–50, 63–68, Springer.

Sato, K. and T.J. Dunkerton, 1997: Estimates of momentum flux associated with equatorial Kelvin and gravity waves. J. Geophys. Res., CADRE issue (in press).

Sato, K. and F. Hasegawa and I. Hirota, 1994: Short-period disturbances in the equatorial lower stratosphere. J. Meteor. Soc. Japan, 72, 859–872.

Takahashi, M., 1996: Simulation of the stratospheric quasi-biennial oscillation using a general circulation model. Geophys. Res. Letters, 23, 661–664.

Takahashi, M., N. Zhao and T. Kumakura, 1997: Equatorial waves in a general circulation model simulating a quasi-biennial oscillation. J. Meteor. Soc. Japan, 75, 529–540.

Takayabu, Y.N., 1994a: Large-scale cloud disturbances associated with equatorial waves. Part I: Spectral feature of the cloud disturbances. J. Meteor. Soc. Japan, 72. 433–449.

Takayabu, Y.N., 1994b: Large-scale cloud disturbances associated with equatorial waves. Part II: Westward-propagating inertio-gravity waves. J. Meteor. Soc. Japan, 72. 451–465.

Wallace, J.M. and V.E. Kousky, 1968: Observational evidence of Kelvin waves in the tropical stratosphere. J. Atmos. Sci., 25, 280–292.

Yanai, M. and T. Maruyama, 1966: Stratospheric wave disturbances propagating over the equatorial Pacific. J. Meteor. Soc. Japan., 44, 291–294.

水平分解能の高いSKYHI大循環モデルに現れる熱帯重力波とスーパークラスター

林　良一 ・ D.G. Golder

（プリンストン地球流体研究所）

P.W. Jones

（ロス・アラモス国立研究所）

　水平分解能の高い（0.6°経度 × 0.72°緯度、及び 1.0° × 1.2°）40層の GFDL SKYHI 大循環モデルに現れる熱帯重力波とスーパークラスターを低分解能（3.0° × 3.6°）モデル実験による結果と比較した。

　これらのモデルでは、熱帯重力波は降水に伴う熱によって励起されているように思われる。降水はモデルの水平分解能が高い方が、時空間的に局所化され、波数-振動数のスペクトル分布の巾が広くなる。格子間隔規模の降水は、クラウドクラスターに伴う降水に疑似的に対応すると考えられ、更に大規模のスーパークラスターに編成される。クラウドクラスターの西進とスーパークラスターの東進はモデルの水平分解能が高い方がより明瞭に見られる。

　高分解能（0.6° × 0.72°）モデルでは、下部成層圏重力波の運動量フラックスは1日以下の周期成分が主要であることが示される。分解能が（3.0° × 3.6°）から（0.6° × 0.72°）に上がると、この運動量フラックスは倍増する。水平および鉛直分解能が両方ともさらに増加すれば、重力波による運動量フラックス収束が実質的に増え、従って準2年振動が強まることが推測される。